Development of an 18cm Micro Air Vehicle : QUARK

Murat Bronz, Jean-Philippe Condomines, Gautier Hattenberger

Development of an 18cm Micro Air Vehicle : **QUARK**

Murat Bronz,[*] Jean-Philippe Condomines[†]and Gautier Hattenberger[‡]

l'Ecole National de l'Aviation Civile, Toulouse, 31055, France
murat.bronz@enac.fr, jean-philippe.condomines@recherche.enac.fr, gautier.hattenberger@enac.fr

Abstract

This paper describes the development of the **QUARK** micro unmanned air vehicle. The main objective of the study is to show the feasibility of designing an autonomous MAV smaller than $20\,cm$ by using open-source programs and off-the-shelf components. Effort is given to show how to choose the system components and the design variables correctly in order to end up with an optimum design. An open-source multi-disciplinary conceptual aircraft design program called *CDSGN* is used in order to select the appropriate wing planform and the optimum battery capacity. Propeller and electric motor are selected throughout an optimization procedure, which analyze the performance of each suitable off-the-shelf propeller and motor combination for the specific mission requirements of the new design. A $2\,cm \times 2\,cm$ custom autopilot board is specifically designed according to the requirements of the **QUARK**. The modelization of the MEMS sensors (Micro-Electromechanical Systems), that are used on the autopilot, is described and analysed in order to improve the stabilisation and the navigation of the aircraft. Longitdinal dynamics of the vehicle are examined by using an innovative technique, and following that, corresponding flight control gains are tunned prior to the outdoor flight test.

The first prototype has been flown and a smaller $15.9\,cm$ version is designed according to the obtained results. The expected endurance for the final version is over $35\,minutes$ with reaching up to $35\,km$ of range.

1   Introduction

The birth of Micro Air Vehicles goes back to early 1990s, when the RAND Corporation performed a feasibility study. Following that interest, in 1996 Aerovironment showed the feasibility of flying a six-inch MAV in 1996, and later improved the performance of the existing design and performed a 16 minutes of flight in 1997 by manual control. After this achievement, Aerovironment was awarded a DARPA founded Phase II Small Business Innovation Research (SBIR) contract. As a result of this contract, the Black Widow MAV was designed, which is still one of the smallest fixed-wing MAV. Black Widow MAV had 30 minutes of endurance and was able to transmit real-time video to the ground within $1.8\,km$ range. There was an autopilot for stability augmentation, however there was no GPS on-board for autonomous navigation. Recent progresses in the miniaturization of the inertial instruments i.e. Inertial Navigation System (INS) and Global Positioning System (GPS) hardware have led to the design of small, low-cost integrated navigation systems. Despite all these improvements, in the year of 2013, there is no fixed-wing MAV with autonomous navigation capability, which remains a big shortfall. Figure 1 shows INS relative strap-down system cost "projections" as a function of inertial instrument technology and performance.

---

[*]Doctor, Assistant-professor in Applied Aerodynamics, URI-Drones
[†]PhD Candidate in Automatic Control, MAIAA
[‡]Doctor, Assistant-professor in Flight Dynamics, MAIAA

The performance of MEMS-based gyroscopes and accelerometers is significantly affected by complex error characteristics that are stochastics in nature. Therefore, the modelisation of the sensors remains a challenge in order to improve the navigation.
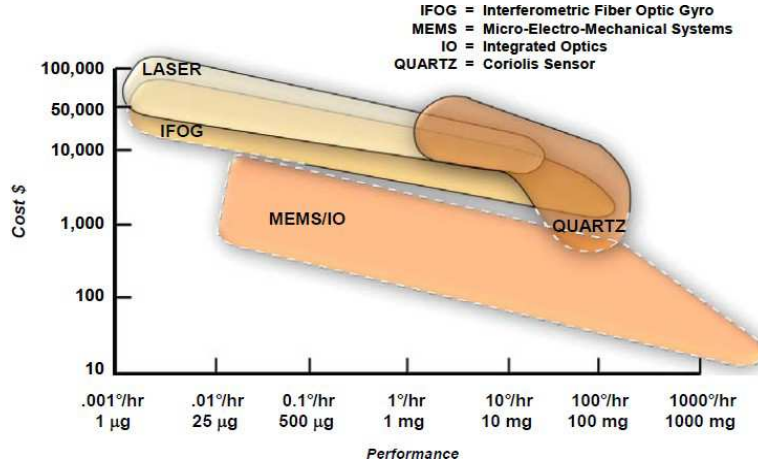

Figure 1: Strapdown INS cost as a function of instrument technology

On the rotary-wing MAVs, the Black Hornet MAV from Proxy Dynamics, demonstrated the state of the art for MAVs with autonomous navigation capability. The current study presents the development of the **QUARK** MAV, starting with the parametric and multi-disciplinary conceptual design phase in cooperation with propulsion system optimization.

2 Design Methodology

The design method was kept simple. The idea was to gather the most appropriate off-the-shelf components that are required for the flight, control, and communication of the aircraft and decide the minimum core size while taking into account the interference and center of gravity issues. Then by using a multi-disciplinary parametric conceptual design program called *CDSGN* [2], the wing planform, battery capacity, cruise speed, motor and propeller combination was optimized while the cost function being the endurance and range performance maximisation. Certain stability derivatives, such as pitch damping (C_{m_q}) and spiral stability ($C_{l_b}C_{n_r}/C_{l_r}C_{n_b}$), are used as constraints during the optimization phase.

3 Off-the-Shelf Component Search

One of the main objectives of this study was to use completely off-the-shelf commercially available components for the realization of the aircraft.

Mini-micro Scale Propellers. Among the available mini-micro scale propellers, seven different candidates were found and taken into consideration for the final propulsion system selection. Figure 2 shows the pictures and Table 1 presents the specifications of the candidate propellers. Each of the propellers modelled geometrically by measuring their chord length, and twist angle at several sections

throhout the blade span. The corresponding airfoil geometry is extracted by cutting the propeller blade into pieces and then aerodynamic characteristics of each section airfoil is examined by using XFOIL[3]. Following that, the performance modelisation of the propellers done by using QPROP[4].

Figure 2: Pictures of candidtae commercially available off-the-shelf mini and micro propellers

Propeller Name	Blade number	Diameter	Pitch	Mass
	[-]	[inch]	[inch]	[g]
Three Blade Prop	3	3.8	-	1.9
Graupner CAM Slim	2	3	3	0.8
Graupner CAM Speed	2	4	3	0.95
GEMFAN mini 3x2	2	3	2	1.0
GEMFAN mini 4x2.5	2	4	2.5	1.4
Red propeller	2	3	-	0.7
HobbyKing nano prop	2	2.2	-	0.3

Table 1: Coefficients of candidate commercially available off-the-shelf mini and micro electric motors

Micro Electric Motors.   Likewise a micro electric motor database was created from the commercially available off-the-shelf motors. Figure 3 shows the candidate electric motors. A first order electric model is used to characterize the behavior of the motors. Only the internal resistance ($\mathcal{R}_m$), no-load current (I_0), and speed constant (K_v) are used for characterization. Table 2 presents the mass of each motor with their K_v coefficient.

4   Design Parametrization

Once the required electronics was defined, the sizing of the aircraft has taken into consideration in a parametric way, which starts with the minimum possible dimension of the internal components and goes up to the user defined maximum limits. The optmization was done by using *CDSGN* program
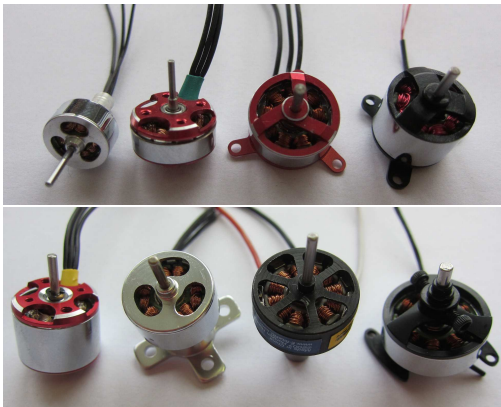

Figure 3: Pictures of candidate commercially available off-the-shelf mini and micro electric motors

Motor Name	Mass	Kv
	[g]	[rpm/V]
1404N	9.2	2290
E-Flite Park 180	8.0	2200
ADH50XL	7.5	1700
HK AP05	5.8	3000
HexTronik 5g	5.0	2000
A05	4.3	2900
ADH30S	2.7	7500
HexTronik 2g	2.0	7700

Table 2: Coefficients of candidate commercially available off-the-shelf mini and micro electric motors
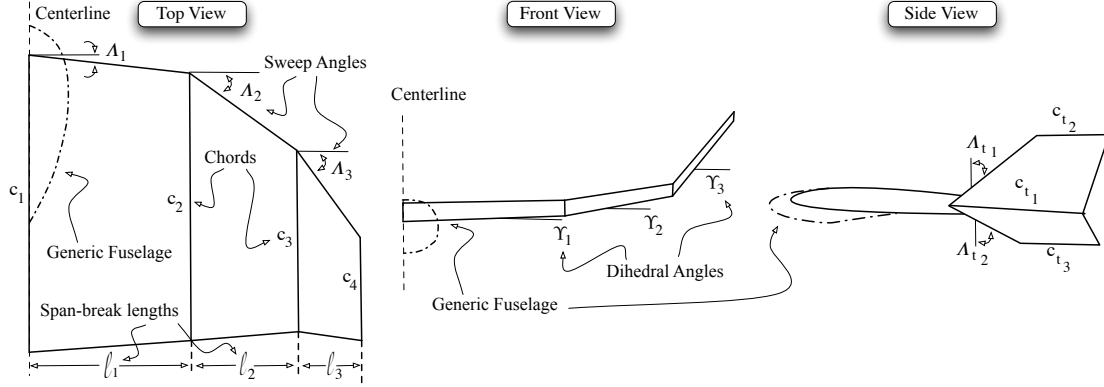
Figure 4: Main parameters for the wing planform that were variable during the multi-disciplinary optimization of the **QUARK** MAV by *CDSGN* program

through changing the wing planform (plus the vertical component of the wing), battery capacity, and cruise speed for candidate motor and propeller combinations. Figure 4 shows the main parameters that were variable for the wing planform while optimizing performance of the QUARK MAV.

5 System Integration and Design

It is crucial to take into account the system integration during the design phase. Finally, the limitation on the battery shape, servo choice and GPS module (because of their availability and ordering issues by a research lab) restricted the minimum dimensions of the parameters and created a solid core system that has to be fitted into the vehicle. According to the center of gravity and the wing thickness issues, the placement of the components have been fixed without too much option. Figure 9 shows the internal placement of the components in the final design. Note that the requirement of placing every component as close as possible to the leading edge comes from the center of gravity alignment. Figure 5 shows the first prototype that is build from EPP foam by using a CNC hot-wire cutting machine and the custom designed smallest Paparazzi autopilot for the **QUARK** MAV.

6 Sensor modelling

All the sensors embedded in the Quark autopilot are low-cost and so have imperfection. The major error sources in the navigation system are due to : -the inertial instrument imperfections (the sensor itself); -the numerical integration process in the INS mechanization. Inertial sensors have both deterministic and random errors. Deterministic errors are due to manufacturing (characteristized by the manufactuers and generally over-estimated with respect to effective values [1]) and mounting defects. This can be obtained using calibration procedure. On the other hand, the stochastic errors are random errors that occur due to random variations of bias or scale factor over time. The accurate modeling of the MEMS sensor errors is one of the most challenging tasks in the design of low-cost navigation. Indeed, to overcome the disadvantages associated with autonomous operation of the GPS and INS, the two systems are often paired together and the INS/GPS data fusion is commonly permormed using Kalman Filter (KF)[5]. There are more recent derivatives of KF known as GMEKF[8] and π-IUKF

4

Figure 5: The prototype **QUARK** MAV wit the new developed **QUARK** Paparazzi Autopilot (October 2012)

[7]. KF has widely been used for data fusion but there are, however some inadequacies, including the following :

- the requirement for a priori information of the system and measurement covariance matrices, R and Q, for each sensor;

- the necessity to have a gaussian assumption on probability distribution and a white bandwith noise.

A general model for the sensor output can be described by the following equation [9] :

$$\zeta_m = (1 + S_f)\zeta_t + b(t) + n(t) \tag{1}$$

where ζ_m is the mesured quality at the sensor output and ζ_t is the true quatity. S_f represent scale factor error (In this work, we will ignore the scale factor error $S_f = 0$ i.e, calibrated out at the factory), $b(t)$ represents the time varying bias (random drift) and $n(t)$ is observation noise, which is assumed to be band limited white noise with spectral density R. This can be characterized by taking the standard deviation of the sensor's output over a short period of time with no input applied. The bias term $b(t)$ is a random process consisting of the integral of a white noise process $\omega(t)$ with spectral density Q. The bias signal is modeled as follows :

$$\dot{b}(t) = \omega_b, \quad E\{\omega(t_1)\omega(t_2)\} = Q\delta(t_1 - t_2) \tag{2}$$

	Static Bias	σ	$R = \sqrt{\sigma^2 \cdot dt}$	R (datasheet)	Q	GPS	σ	
X-acceleration	0.142	0.0319	1000	400	$9.09e^{-5}$	X	0.88	m
Y-acceleration	-0.3	0.0985	3100	400	$7.26e^{-5}$	Y	1.45	m
Z-acceleration	0.19	0.049	1600	400	$4.02e^{-4}$	Z	20.29	m
Roll	-1.55	0.0825	0.0082	0.0224	$3.6e^{-3}$	V_X	0.248	m/s
Pitch	-1.13	0.1673	0.016	0.0224	$19\ e^{-3}$	V_Y	0.146	m/s
Yaw	-1.7	0.2214	0.047	0.0224	$1.9\ e^{-3}$	V_Z	0.280	m/s

Table 3: Covariance and static error for INS sensors   Table 4: GPS variance

In order to extract the covariance and static bias of each sensor noise afecting the ouput, we have analyzed 1000 samples of each sensor using a PDF (Probability Density Function). These data

coming from hight frequency dataloger system working at 100 Hz (dt=0.01s) for INS sensor and 5 Hz (dt=0.2s) for GPS. Remark that, a simplest Allan variance analysis[6] with a record of 2 hours of data has been conducted to obtain spectral density Q. The determined models for each of the sensors (gyrometers and accelerometers) are tabulated in Table 3, and shows that spectral density values R (μg or $^{\circ}/s/\sqrt{(Hz)}$) given by the manufacturer are generally overestimated or underestimated with respect to effective values. For example, a spectral density value of $0.0082^{\circ}/s/\sqrt{(Hz)} = (0.0082 \cdot 60)^{\circ}/\sqrt{(hr)}$ on the roll axis rotation rate indicates, that the angular error (incertainty) due to random walk is e.g. 0.063 deg after 1minute or 3.8 deg after 1hour. The first two column represents static bias and standard deviation (σ) and the last column Q represents spectral density of $\omega(t)$ coming from Allan variance analysis. In terms of visual comparison, only gyrometers histogram are shown in Fig.N, and match with a gaussian distribution. Note that it is the same shape for accelerometers histogram. Finally, GPS data variance are tabulated in Table 4 for speed and position.
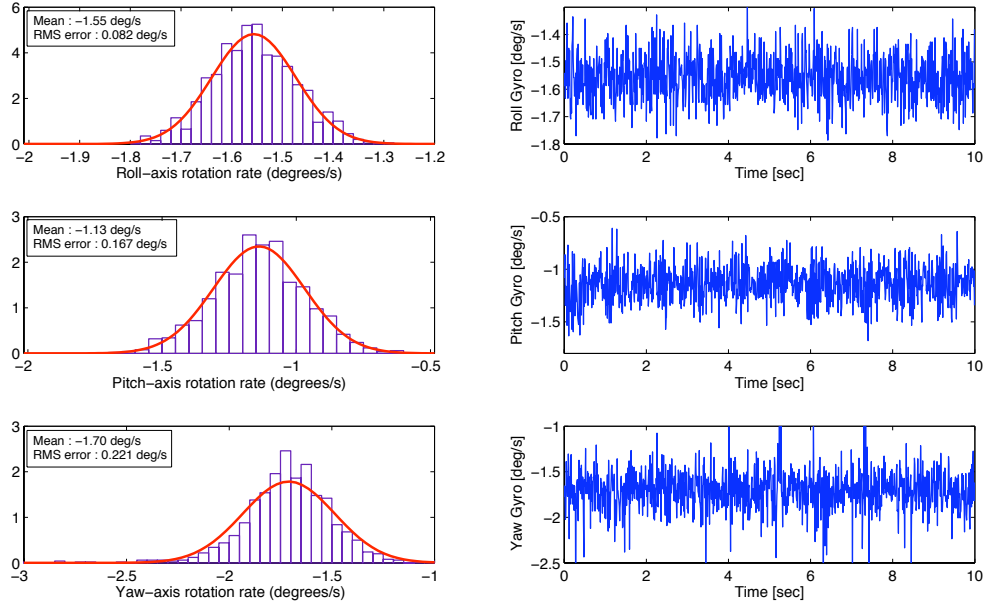

Figure 6: Distribution and RMS error of the used gyrometer

Inertial sensor always contain a certain amount of measurement noise (e.g, vibration). On the sensor level, this noise is usually separated into long-term (low-frequency) and short-term (high-frequency) noise. Wavelet denoising is frequently used to process inertial sensors measurements to improve the signal-to-noise ratio (SNR). However, in the case of **QUARK** Paparazzi autopilot, it will not be possible to use wavelet denoising because it is computationally costly. Frequency Fourier Transformation (FFT) of both gyrometer and accelerometer, recorded with an on-board datalogging system, for main flight phases (waiting, takeoff, cruise an landing) are represented in Figure 7. FFT which depends on the throttle, shows similar characteristics on both sensors after 20 Hz which can be considered as vibration noise. Thus, a Low Pass Filter (LPF) with a cut frequency at 22 Hz can be used to remove high frequency vibration. This LPF has been implemented to the autopilot.
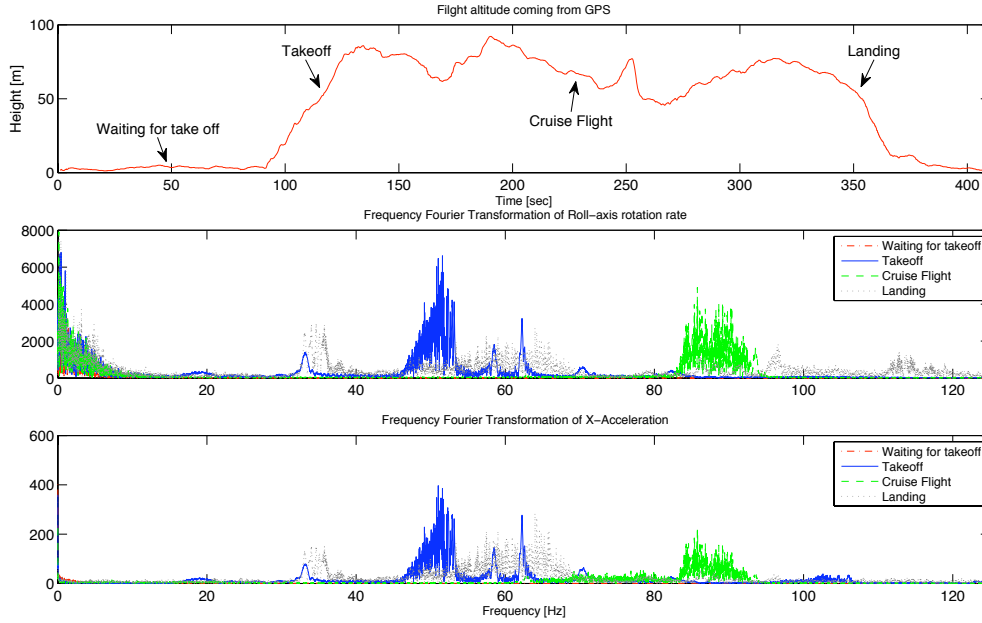
Figure 7: Frequency Fourier Transformation of roll-axis gyrometer and X-axis accelerometer values with the flight altitude information on the top.

7 Flight Tests

7.1 Longitudinal Tuning

The difficulty of flying such a small aircraft is obvious, so that prior to the outdoor flight tests, it is decided to tune the longitudinal control loop gains with a restricted flight method, that is shown in Figure 8, and tune the longitudinal control loop gains prior to the maiden flight.
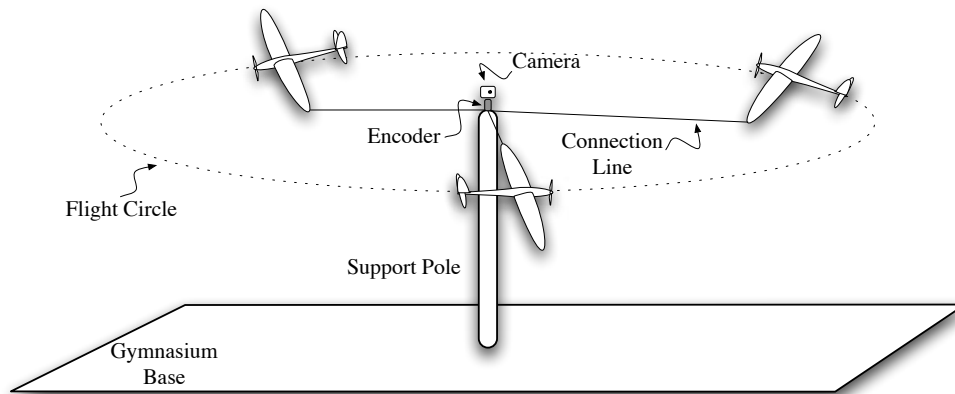
Figure 8: The longitudinal control test setup for restricted flight tests

The experiment is done in a closed place, where a pole is used as the center fixation point. The aircraft is connected from its wing-tip to an encoder which is placed on top of the fixation pole. The encoder was turning freely and measuring the exact rotation rate during the experiment. Additionally, a high frame rate camera is placed on top of the encoder directed to the aircraft which will be recording the vertical movement of the aircraft during the flight with a fixed reference.

The length of the line has been increased gradually. The center of gravity was located at aircraft's aerodynamic center because of component integration issues resulting a highly agile vehicle. Therefore, the experiment started directly with autopilot assisted mode where the pilot controls the attitude of the vehicle through autopilot (fly-by-wire). The longitudinal control loop gains tuned while watching the oscillation of the vehicle and the line length has been increased up to the wall limits.

As a result of the experiment, several important flight parameters are obtained such as, the longitudinal control loop gains, the minimum flight speed, approximate cruise throttle setting, flight angle of attack at different speeds. Additionally, the control surface travels obtained for the pitch control have been copied for the roll control travels as a starting point for the outdoor flight.

7.2   Outdoor Flights

The first parameters and gains that are obtained from the pole flight tests are applied for the maiden flight. The flight has been started directly in autopilot assisted mode as explained in the previous section. After a short attempt, a small angle of attack increment was required in order to sustain the level flight. The pitch proportional gains has been increased (10%) in comparison to the values that are obtained from the pole flight tests. However the lateral behavior of the vehicle was satisfactory directly from the beginning (in no-wind condition). Although the maiden flight took less then 5 minutes, the amount of battery energy used for the flight gives an estimated 20 minutes of flight time for the current prototype with small batteries.

The second flight has been made in a windy day with more than $10\,m/s$ wind gusts. The main objective of this flight was to tune the navigation control loop gains in order to fly completely autonomously. Unfortunately, $20\,m$ after the launch the telemetry link started to degrade and as the safety pilot radio command link was transmitted through the telemetry, it was no more possible to take back the flight control of the vehicle. However, the starting navigation control loops were sufficient enough to keep the vehicle in the air following the predefined flight circle on top of experiment area. Therefore, we had the chance to change some of the stabilisation and navigation control gains whenever we catch telemetry connection.We have observed severe rolls because of the strong wind gusts several times, and the counter force applied in order to correct them was seemed to be not sufficient and fast enough. That leads us to increase the lateral gains which should theoretically improve the response for the wind-gusts, unfortunately before being able to change and tune the gains (lack of constant communication), the vehicle crashed because of a strong wind gust. Thanks to its light weight and low inertia, beside a broken propeller there was no other major damage.

The third flight has been made in calm weather conditions with some modifications to the telemetry link with the hopes of improved the communication. Unfortunately, the telemetry behavior was the same as the previous flight limiting the further tuning of the vehicle. As the weather was calm with less wind, the vehicle flew much better and follow the desired trajectory closely compared to the previous flight. After 5 minutes of autonomous flight, the plane started to loose altitude at a point of the trajectory where the communication was lost. It finally crashed in a field where it was not possible to retrieve it. Without any telemetry data, the reason for this crash remain unknown.

Despite having lost the only prototype, we have obtained precious information from the flights. The prototype showed the feasibility of flying smaller than $20\,cm$ vehicle with cheap off-the-shelf

components. It was also a good opportunity to verify and correct our aerodynamic codes for this scale which gives a big confidence for the future designs.

8   On-going Work

According to the experience gained from the prototype design and flights, a new version of the **QUARK** MAV is designed with $15.9\,cm$ wing span. This time the manufacturing of the vehicle is going to be done by using precisely machined molds by CNC. The total take-off weight is $67\,g$. Figure 9 shows the CAD model of the new **QUARK** with the already manufactured aluminium molds.
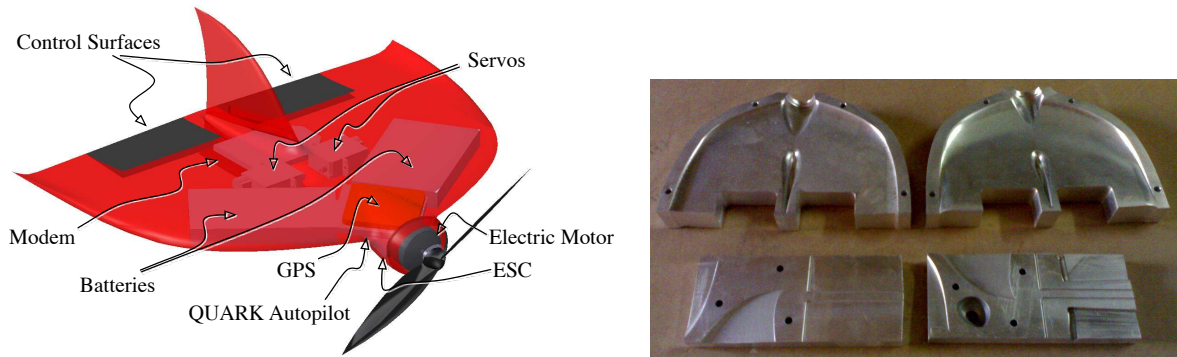

Figure 9: The CAD representation of the final **QUARK** MAV with the internal components and the aluminium CNC molds on the right

As a continuation and future work of this study, the telemetry integration will be taken into consideration more seriously in order to improve the communication. Additionally in order to make this scale of MAVs useful for real-life applications such as surveillance and information gathering from an hazardous place, a micro camera and its transmitter will be integrated into system. The camera integration has been already included on the final **QUARK** design.

9   Conclusion

Present work explains the efforts given for the realisation of an MAV with a maximum size of smaller than $20\,cm$. The first prototype ($18\,cm$) is designed and manufactured by using off-the-shelf components. Complete autonomous flight including stabilisation and navigation has been achieved with the prototype. The results obtained from the limited number of flights shows a good confidence for the final design ($15.9\,cm$) to fly over 35 minutes at a flight speed of $15\,m/s$ and reach up to $30\,km$ for the straight line range at a speed of $16\,m/s$.

Acknowledgements

References

[1] Mattia De Agostino, Ambrogi Maria Manzino, and Marco Piras. Performance Comparison of Different MEMS-based IMUs. In *Position Location and Navigation Symposium (PLANS) 2013 IEEE/ON*, may 2010.

[2] Murat Bronz. *A Contribution to the Design of Long-Endurance Mini Aerial Vehicles*. PhD thesis, l'Ecole National de l'Aviation Civile, 2012.

[3] Mark Drela. An analysis and design system for low reynolds number airfoils. In University of Notre Dame, editor, *Conference on Low Reynolds Number Airfoil Aerodynamics*, June 1989.

[4] Mark Drela. *QPROP Formulation*. MIT Aero and Astro, June 2006.

[5] Kalman R. E. A new approach to linear filtering and prediction problems. *Journal of basic Engineering*, 82(1):35–45, 1960.

[6] El-Sheimy N., Hou H., and Niu X. Analysis and modeling of inertial sensors using allan variance. *IEEE Transactions on Instrumentation and Measurement*, 57(1):140–149, 2008.

[7] Condomines J. P., Seren C., and Hattenberger G. Nonlinear state estimation using an invariant unscented kalman filter. In *AIAA Guidance Navigation and Control Conference*, pages 1–15, Boston, MA, August 2013.

[8] Martin P. and Salaün E. Generalized multiplicative extended kalman filter for aided attitude and heading reference system. In *AIAA Guidance Navigation and Control Conference*, pages 1–13, August 2010.

[9] L. Wenger and D. Gebre Egziabher. Systems Concepts and Performances Analysis of Multi-Sensor Navigation System for UAV Applications. In *2nd AIAA Unmanned Unlimited Systems Conference, San Diego, CA, AIAA*, 2003.